Medial Axis Approximation and Unstable Flow Complex

Joachim Giesen* Edgar A. Ramos† Bardia Sadri‡

January 2, 2010

Abstract

The medial axis of a shape is known to carry a lot of information about the shape. In particular, a recent result of Lieutier establishes that every bounded open subset of $\mathbb{R}^n$ has the same homotopy type as its medial axis. In this paper we provide an algorithm that computes a structure we call the *core* for the approximation of the medial axis of a shape with smooth boundary from a discrete sample of its boundary. The core is a piecewise linear cell complex that is guaranteed to capture the topology of the medial axis of the shape provided the sample of its boundary is sufficiently dense but not necessarily uniform. We also present a natural method for augmenting the core in order to extend it geometrically while maintaining the topological guarantees. The definition of the core and its extension are based on the steepest ascent flow map that results from the distance function induced by the sample point set. We also provide a geometric guarantee on the closeness of the core and the actual medial axis.

1 Introduction

The medial axis of a bounded open set S in $\mathbb{R}^n$ is the set of points in S with at least two closest points in the boundary of S. In the following we sometimes refer to bounded open subsets of $\mathbb{R}^n$ as *shapes*. A recent result of Lieutier [16] establishes that any shape and its medial axis have the same topological type or, more precisely, are homotopy equivalent. Consequently, the medial axis can be used to answer topological queries about the shape. Such queries are employed in many applications including, but not limited to, shape analysis, motion planning, and mesh partitioning. Therefore, it is sensible to expect any medial axis approximation algorithm to capture the topology of the medial axis.

As a geometric object, the medial axis is unstable since small changes of a shape can cause comparatively large changes in its medial axis. This instability of the medial axis bears two consequences. First, it makes the medial axis hard to compute exactly because of numerical instabilities; consequently, exact computation of medial axis has only been attempted for a few limited classes of shapes, see for example [7]. Second, the complete medial axis may be less interesting in practice than an approximation of it which carries the same topological type but is more stable under small perturbations of the shape. Approximations of the medial axis of a shape are often sought with a sample of the boundary of the shape provided as input. Chazal and Lieutier [8] defined the λ-medial axis, a subset of the medial axis, which has the desired stability, and is guaranteed to have the same homotopy type as the medial axis for suitably small values of the parameter λ. The largest

*Max-Planck Institut für Informatik, Research partly supported the Swiss National Foundation under the project "Non-linear manifold learning".

†University of Illinois

‡Duke University

topologically safe value of λ depends on the shape and can be very small and hard to determine [3]. Finally, the existing algorithm for computing the λ-medial axis requires a very dense *uniform* sample of the boundary of the shape [8].

The ε-sampling theory of Amenta and Bern [1] provides a framework for the analysis of algorithms that either reconstruct the boundary of a shape or approximate its medial axis. The local density of an *adaptive* ε-sample in this framework may vary but is guaranteed to adapt locally to the features of the shape. Several results were obtained in this framework, some of the earliest concerning the medial axis are due to Amenta, Bern, and Eppstein [2], and Boissonnat and Cazals [5], each establishing that a subset of the Voronoi vertices in the Voronoi diagram of the sample points lies close to the medial axis. Later, Amenta, Choi, and Kolluri [4] designed an algorithm that computes an approximation of the medial axis, in the form of a cell complex, that is provably homotopy equivalent to the medial axis of the shape, provided that that shape boundary is sampled densely enough. The output of this algorithm tends to be noisy and needs to be cleaned up using heuristics for practical use. The cell complex produced by this algorithm is not contained in the Voronoi 2-skeleton of the sample points, a property considered natural since the Voronoi 2-skeleton is the medial axis of the sample points and that effective filtering of it often produces good results in practice. Dey and Zhao [10] designed an algorithm that outputs a sub-complex of the Voronoi 2-skeleton for medial axis approximation. The geometrically pleasing output of this algorithm is guaranteed to converge to the true medial axis when the sample grows infinitely dense, i.e., when $\varepsilon \to 0$, but suffers lacking of any topological guarantees. In fact, with a poor choice of filtering parameters the provided output can be flawed topologically. The results of the present paper can be used to mend this deficiency.

Our Contributions Given a sample of the surface of a shape, we compute a piece-wise linear cell complex, which we call the *core* (of the medial axis approximation). The core is extracted from a refinement of the Voronoi 2-skeleton of the input sample called the *unstable flow complex*. The idea and the algorithm to compute this complex and the core are derived from the critical point theory of the distance function to the sample points and their induced steepest ascent flow, which we refer to as the *discrete flow*.

We analyze the properties of the core in the Amenta-Bern framework. Dey et al. [9] show that the critical points of the distance function to an ε-sampling of the boundary of a shape are naturally separated: each such critical point is either very close to the surface or very close to the medial axis of the shape. The two classes of critical points can be separated algorithmically provided that the sample is sufficiently dense. The core we compute is the union of the *unstable manifolds* of the critical points close to the medial axis. The unstable manifold of a critical point consists of all points that can be reached from an infinitesimally small neighborhood of that critical point following the discrete flow. We characterize the structure of the unstable manifolds and show how to compute them from the Voronoi complex of the sample points in $\mathbb{R}^3$. Our main result states that the core and the medial axis are homotopy equivalent for dense enough samples.

Once the core is computed, it can be extended to better capture the geometry of the medial axis while maintaining its homotopy type. To extend the core one picks, using any algorithm at hand, a set of points that approximates a subset of the medial axis of the target shape and adds this set to the computed core along with its *flow closure* under the discrete flow. We show that as long as the chosen approximating set of points does not get too close to the surface of the shape, adding the closure keeps the homotopy type of the core. Because of this property, computing the core can be used to augment most medial axis approximation algorithm into a topologically accurate one. The algorithm of Dey and Zhao [10] is especially suited for augmenting the core since computing

the flow closure of Voronoi facets is easy.

Finally we provide an upper-bound on the rate at which the distance of a point to the medial axis can grow as the point moves along its flow line in the discrete flow. This shows that the discrete flow closure of points near the medial axis does not escape the medial axis rapidly. One consequence of such a geometric guarantee is that the core gets closer and closer to the medial axis and is contained in it at the limit as $\varepsilon \to 0$. Moreover, if the core is extended using a set that converges to the real medial axis when $\varepsilon \to 0$, such as the Voronoi facets filtered by the algorithm of Dey and Zhao, then the extended core also converges to the real medial axis in Hausdorff distance all the while staying homotopy equivalent to it.

The structure of the paper is as follows. In Section 2 we introduce basic definitions and state some known results. Section 3 establishes several homotopy equivalences , most importantly the homotopy equivalence of the medial axis, the core, and the extended core. Section 4 describes how to provide geometric guarantees for the core and flow closures. In Section 5 we present algorithms for computing the unstable flow complex, the core, and flow closures of Voronoi faces. Concluding remarks and experimental results are provided in Section 6.

2 Preliminaries

In this section we review some basic definitions as well as some required background material. It is important to note that although we present all the definitions for $\mathbb{R}^3$, all the statements and results of the present section as well as those in Sections 3 and 4 generalize to higher dimensional Euclidean spaces. Only the algorithms presented in Section 5 are designed specifically for $\mathbb{R}^3$.

Basic Notions For a point $x \in \mathbb{R}^3$ and $r > 0$, we denote by $B(x, r)$ the open ball of radius r centered at x, i.e., $B(x, r) = \{y \in \mathbb{R}^3 : \|x - y\| < r\}$, and by $\overline{B}(x, r)$ the closure of $B(x, r)$, i.e., $\overline{B}(x, r) = \{y \in \mathbb{R}^3 : \|x - y\| \leq r\}$. We also refer to $B(x, r)$ as the *r-neighborhood* of x. For $x \in \mathbb{R}^3$ and any subset $S \subset \mathbb{R}^3$, we define the distance between x and S as $\text{dist}(x, S) = \inf_{y \in S} \|x - y\|$. By S^c we denote the complement of S in $\mathbb{R}^3$.

Surface, Shape and Medial Axis We consider smooth closed connected orientable 2-manifolds embedded in $\mathbb{R}^3$. We call such manifolds *surfaces*. Throughout, our *target* surfaces, from which the sample is taken, is denoted by Σ. Any surface Σ is associated with the two *open* components of its complement Σ^c. One of these two components is bounded and the other one unbounded. We sometimes call the former the *inner* component or shape and the latter the *outer* component of the surface. When referring to our target surface Σ, the inner component is denoted by S and the outer one by S^*. The *medial axis* $M(S)$ of the open set S is the set of all points in S that have at least two closest points in Σ, i.e., $M(S) = \{x \in S : |A_S(x)| > 1\}$, where $A_S(x)$ is the set of closest points to x in Σ, i.e. $A_S(x) = \{y \in \partial S : \|x - y\| = \text{dist}(x, \partial S)\}$. Note that since Σ is compact, $A_S(x)$ is well-defined and non-empty for every $x \in S$. The medial axis $M(\Sigma)$ of a surface Σ is the union of the medial axes of the inner and outer components S and S^* associated to Σ, i.e., $M(\Sigma) = M(S) \cup M(S^*)$. We also call $M(S)$ and $M(S^*)$ the *inner* and the *outer*, respectively, medial axis of Σ. Thus, $M(\Sigma)$ consists of all points in $\mathbb{R}^3$ that have at least two closest points in Σ. In what follows, M represents the medial axis $M(\Sigma)$ of our target surface Σ.

Feature Size and Surface Samples By definition, every point of M^c has a unique closest point in Σ. For any point $x \in (\Sigma \cup M)^c$ we denote by $\hat{x}$ the unique closest surface point to x, i.e.,

$\hat{x} = \text{argmin}_{y\in\Sigma}\|x-y\|$, and by $\check{x} \in M$ we denote the center of the medial ball tangent to Σ at $\hat{x}$ and at the same side of Σ as x. The *medial feature size* is the function $\mu : (\Sigma \cup M)^c \to \mathbb{R} \cup \{\infty\}$ defined as $\mu(x) = \|\hat{x}-\check{x}\|$. The function $f : \Sigma \to \mathbb{R}, x \mapsto \inf_{y\in M} \|x-y\|$, which assigns to each point in Σ its distance to the medial axis M, is called the *local feature size*. Note that for $x \in (\Sigma \cup M)^c$ it always holds that $f(\hat{x}) \leq \mu(x)$. It can also be easily seen that f is 1-Lipschitz, i.e. for every $x, y \in \Sigma$, $|f(x) - f(y)| \leq \|x - y\|$. Throughout this paper, we assume that every point $x \in \Sigma$ has non-zero local feature size and that the infimum of the local feature size function over Σ, $f_0 = \inf_{x\in\Sigma} f(x)$, sometimes called the *reach* of Σ is bounded away from zero.

For a constant $\varepsilon > 0$, a finite sample $P \subset \Sigma$ is called an ε-sample if for all $x \in \Sigma$, there exists a sample point $p \in P$ within distance $\varepsilon f(x)$ from x.

Distance Functions and Derived Concepts Given an open set, S we define the *distance function* h_S induced by S as

$$h_S(x) : S \to \mathbb{R}, \quad x \mapsto \text{dist}(x, S^c).$$

If S is a shape enclosed by a surface Σ, then $h_S(x) = \text{dist}(x, \Sigma)$ and we can expand the domain of the function to the entire $\mathbb{R}^3$ and denote it by h_Σ. Distance functions have been extensively studied in the literature (see for example [13]) and are known to carry a great deal of information about the sets inducing them. For example, Σ itself is simply given by $h_\Sigma^{-1}(0)$ and the medial axis M of Σ turns out to consist of all points in Σ^c at which h_Σ is not differentiable. In the context of this paper where our understanding of the target surface Σ is limited to a discrete ε-sample P of it, we aim at extracting similar information from the distance function induced by P, h_P. The latter function is in a sense an approximation of h_Σ.

The function h_S (also h_Σ and more generally any distance function) is 1-Lipschitz and therefore continuous. However, it is not differentiable everywhere in S and in particular ∇h_S is undefined over a certain subset of S. As mentioned above, this subset is precisely the medial axis $M(S)$ of S. Nevertheless, a unique direction of steepest ascent for h_S exists and can be determined everywhere in S except for a set of isolated *critical points* of h_S [13]. A vector field v_S can then be characterized everywhere in S that agrees whit this direction of steepest ascent at every non-critical (or *regular*) point of h_S and vanishes at critical points. Furthermore, v_S agrees with ∇h_S on $S \setminus M(S)$ where the latter is defined. A critical point of h_S is a point $x \in S$ that is contained in the convex hull of $A_S(x)$. Every other point of S is regular.

In order to characterize the vector field v_S at a point $x \in S$, let $d_S(x)$ be the center of the smallest enclosing ball of $A_S(x)$ and let $r_S(x)$ be its radius (Figure 1). We define the *flow vector* at x (with respect to S) as

$$v_S(x) = \frac{x - d_S(x)}{h_S(x)}.$$

The vector $v_S(x)$ agrees with $\nabla h_S(x)$ at every point $x \in S$ for which this gradient is defined and extends the gradient of h_S everywhere else by determining the direction of steepest ascent for h_S [16]. The points x for which $v_S(x) = 0$ are exactly the critical points of h_S. It can be easily verified using Pythagoras's theorem that

$$\|v_S(x)\|^2 = 1 - \left(\frac{r_S(x)}{h_S(x)}\right)^2. \tag{1}$$

By showing the convergence of Euler schemes, Lieutier [16] proved that for any *bounded open* set S, the flow vector field v_S as described above can be integrated, to give a flow map ϕ_S :

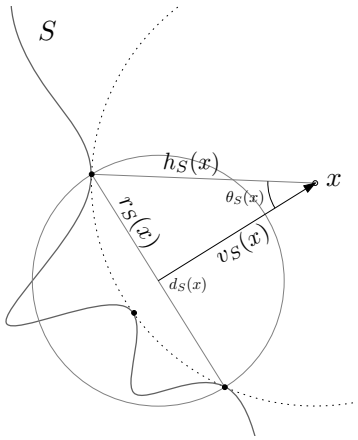

Figure 1: Characterization of the steepest ascent direction for a point $x \in S$. Solid points on the boundary of S represent $A_S(x)$.

$\mathbb{R}^+ \times S \to S$ that is continuous in *both* variables and satisfies for all $x \in S$: *(1)* $\phi_S(0, x) = x$ and *(2)* $\phi_S(s, \phi_S(t, x)) = \phi_S(s + t, x)$ for all $s, t \in \mathbb{R}^+$.

Starting at any point $x \in S$, the flow map $t \mapsto \phi_S(t, x)$ defines a continuous path in S, called the *orbit* of x and denoted $\phi_S(x)$, where t varies from 0 to $+\infty$. In other words,

$$\phi_S(x) = \{\phi_S(t, x) : t \in [0, \infty]\}.$$

More generally, for any set T, we define the orbit of T as the union of orbits of the points in T, i.e.

$$\phi_S(T) = \bigcup_{x \in T} \phi_S(x).$$

At any point $y = \phi_S(t, x)$ the flow vector $v_S(y)$ determines the direction of the flow at y. Lieutier further proved that when S is a bounded open set then for any point $x \in S$ both of the maps $t \mapsto h_S(\phi_S(t, x))$ and $t \mapsto r_S(\phi_S(t, x))$ are increasing and that the former map is continuous and satisfies the following integral equation:

$$h_S(\phi_S(t, x)) = h_S(x) + \int_0^t \|v_S(\phi_S(\tau, x))\|^2 d\tau. \tag{2}$$

It turns out that the critical points of h_S are the fixed points of the flow map, i.e., if c is a critical point of h_S, then $\phi_S(t, c) = c$ for all $t \in \mathbb{R}^+$.

As motivated above, given a sample P of Σ, it is natural to try to compare the distance function h_S with the function

$$h_P : \mathbb{R}^3 \to \mathbb{R}, \qquad x \mapsto \min_{p \in P} \|x - p\|,$$

that assigns to each point its distance to the sample P of Σ. The finite set P is the boundary of the open set $P^c = \mathbb{R}^3 \setminus P$ and we can define the distance function h_{P^c} and the corresponding flow vector field ϕ_{P^c} induced by P^c as we did for S. Since h_{P^c} and h_P are exactly the same function, in a slight abuse of notation we will denote both of these distance function with h_P and let

$$A_P(x) = \{y \in P \mid \|x - y\| = h_P(x)\}.$$

We shall also denote the center of the smallest ball containing $A_P(x)$ as $d_P(x)$ and the associated flow vector field as v_P. Note that $d_P(x)$ is the closest point on the Delaunay face dual to the lowest dimensional Voronoi face that contains x. Sometimes $d_P(x)$ is referred to as the *driver* of x. Technically speaking, since P^c is unbounded, h_P has a critical point (a maximum) at infinity. All other critical points of h_P can be characterized as the intersection points of Delaunay faces with their dual Voronoi faces [12]. Indeed if $V_P(x)$ denotes the lowest dimensional Voronoi face in $\mathrm{Vor}(P)$, the Voronoi complex defined by P, that contains x and $D_P(x)$ denotes its dual in $\mathrm{Del}(P)$, the Delaunay complex of the same point set, then $\operatorname{conv} A_P(x) = D_P(x)$ and since the affine hulls of $D_P(x)$ and $V_P(x)$ are always orthogonal and therefore intersect in exactly one point, for every critical point c of h_P, we get $\{c\} = D_P(c) \cap V_P(c)$.

Notice that in in the above interpretation of the vector field v_P, we assume that the the Delaunay face $D_P(x)$ and the Voronoi face $V_P(x)$ both contain their relative boundaries and are therefore closed cells. Delaunay cells are indeed compact since they are always bounded. Following [12] we make the *genericity assumption* that if a Voronoi face and its dual intersect, they do so in their relative interiors. In other words, if $V_P(x) \cap D_P(x) = \{c\}$, then c belongs to the relative boundary of neither $V_P(x)$ nor $D_P(x)$. This is indeed a sensible assumption [11] since point-sets P for which this assumption is violated are a measure zero subset of all finite point-sets. In other words, any small perturbation of any point set results a point-set that is generic in the above sense.

It is also helpful to reexamine the definition of the driver of a point for the distance function h_P. As shown by Giesen and John [12], the driver of a point x is the closest point of $D_P(x)$ to x. The orthogonality of affine hulls of $V_P(x)$ and $D_P(x)$ entails that if $V_P(x) = V_P(y)$, then $d_P(x) = d_P(y)$. In particular, all the points in the relative interior of every Voronoi face have the same driver. Consequently, if for a Voronoi face V, the driver of the points in the relative interior of V lies in the affine hull of V, the the restriction of the flow lines of ϕ_P to V are lines segments (or half lines) whose extensions concur at the common driver of the points in V. If on the other hand, the driver is not included in the affine hull of V, then the flow through V moves *transversally* to a coface V' of V. It was shown in [15] that the driver of the points of the relative interior of V' in this case coincide with the driver of those of V. As a result, the flow orbit $\phi_P(x)$ of every point x is a piece-wise linear curve (a polyline) that turns only when it enters the relative interior of new Voronoi face through a proper coface of that face. An important consequence of the map $t \mapsto r_P(\phi_P(t, x))$ being non-decreasing in this case is that no flow line of ϕ_P reaches the same Voronoi faces twice. In other words, any flow line can turn at most as many times as there are Voronoi faces in $\mathrm{Vor}(P)$.

If the shape S is bounded, then the flow orbit $\phi_S(t, x)$ stays inside S. In general, the orbit of a point may converges to a critical (fixed) point h_S, or to a cycle, as $t \to +\infty$. Notice that we include the critical point or the cycle in the flow orbit of x. For a critical point c of the flow ϕ_S, the set of all points x whose flow orbits converges to c is called the *stable manifold* of c and is denoted by $\mathrm{Sm}(c)$. In other words,

$$\mathrm{Sm}(c) = \{x \mid \phi_S(+\infty, x) = c\}.$$

Although there is no flow out of a critical point c of h_S, it is interesting to know where the points very close to c flow. We define the *unstable manifold* $\mathrm{Um}(c)$ of a critical point c, as the set of all points into which points arbitrarily close to c flow. Formally,

$$\mathrm{Um}(c) = \bigcap_{\varepsilon>0} \bigcup_{y \in B(c,\varepsilon)} \phi_S(y).$$

In the special case of h_P, flow orbits are piece-wise linear and cannot enter the same face of $\mathrm{Vor}(P)$ twice. Consequently, flow orbits either reach critical points or go to infinity. In other words, the union of stable manifolds of critical points cover the space.

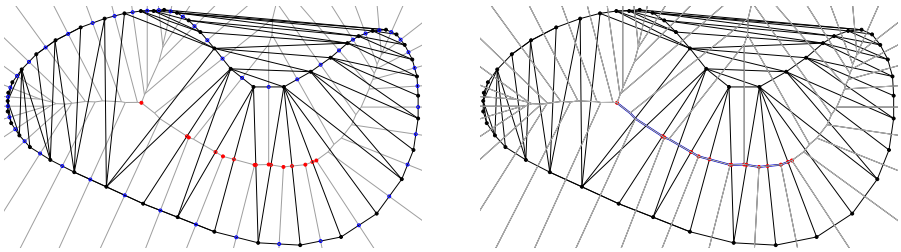

Figure 2: Left: critical points of a sampled curve in $\mathbb{R}^2$. Sample points are index-0 critical points. Index-1 critical points are shown by hollow dots. Surface critical points (other than the sample points) are shown in blue and medial axis critical points in red. Right: the core, i.e. union of unstable manifolds of medial axis critical points, is shown in blue.

Separation of Critical Points Dey, et al. [9] observed that if P is an ε-sample of the smooth boundary Σ of a shape S, then the critical points of the distance function h_P cannot reside everywhere in S. Rather they have to be either very close to Σ or very close to M (Figure 2).

Theorem 2.1 [9] *Let P be an ε-sample of a smooth surface Σ. Then for every critical point c of h_P, either $\|c - \hat{c}\| \leq \varepsilon^2 f(\hat{c})$, or $\|c - \check{c}\| \leq 2\varepsilon\mu(c)$.*

Thus the critical points of h_P can be classified based on whether they are close to Σ or close to M. We refer to the first class of critical points as *surface critical points* and to the second class as *medial axis critical points*. We further subdivide the medial axis critical points h_P into two subgroups: *inner* medial axis critical points are those that are close to $M(S)$ and *outer* medial axis critical points are those close to $M(S^*)$.

Core The union of the unstable manifolds of the inner medial axis critical points of h_P will play an important role in our paper. We refer to this union as the *inner core determined by the sample* P or simply *core* when the determining sample P is clear from the context (Figure 2). We will show that for a sufficiently dense sample P of Σ the core is homotopy equivalent to the medial axis $M(S)$ of the inner shape S.

Unstable Flow Complex We can define a cell complex decomposition of space by grouping together, as cells, the points of the space that are contained in the unstable manifolds of the same set of critical points. We define a relation $\sim$ on the pairs of points in $\mathbb{R}^3$: $x \sim y$ if and only if x is contained in the unstable manifolds of the same set of critical points as y. Obviously $\sim$ is an equivalence relation. The *unstable flow complex* induced by a point set P, denoted $\mathbf{U}(P)$, or just $\mathbf{U}$ when P is understood, is the cell complex whose cells are connected components of the subdivision of space into equivalence classes of the $\sim$ relation. In Section 5 we study the structure of this complex more closely.

3 Homotopy Equivalences

As in the previous section, we always assume that Σ is a connected smooth surface with associated inner and outer components S and S^*. Furthermore, we assume that P is ε-sampling of Σ. Let $\mathcal{C}$ be the *core* as defined in Section 2, i.e., $\mathcal{C}$ is the union of unstable manifolds of the inner medial

axis critical points of the distance function h_P. Here we want to show that $\mathcal{C}$ and the medial axis $M(S)$ of S are homotopy equivalent.

Following Lieutier [16] the following criterion is used throughout this paper to prove homotopy equivalence between topological spaces. For the standard definition of homotopy equivalence see [14].

Proposition 3.1 *Let X and $Y \subseteq X$ be arbitrary sets and let $H : [0,1] \times X \to X$ be a continuous function on both variables satisfying the following three conditions.*

1. $\forall x \in X$, $H(0,x) = x$,
2. $\forall x \in X$, $H(1,x) \in Y$, *and*
3. $\forall y \in Y, \forall t \in [0,1]$, $H(y,t) \in Y$.

Then X and Y have the same homotopy type.

Intuitively, we may interpret the first argument of the map H as time. Using a simple reparameterization in the first argument, we can replace the interval $[0,1]$ with any interval $[0,T]$ where $T > 0$ is a real number. It is important that the time interval considered has finite length. The above criterion for homotopy equivalence between X and Y continuously maps points in X to those in Y during the time interval $[0,T]$. At time 0, all points in X are mapped to themselves and at time T, they have all arrived in Y. Notice, the important property that the points in Y stay in Y all the time.

In the following we want to plug in ϕ_S and ϕ_P (the flow resulted from integrating v_P after circumventing the technical difficulty of unboundedness of P^c) for the map H mentioned above. When distance flow maps are used for H, the first condition of Proposition 3.1 is automatically satisfied since $\phi_S(0,x) = x$ for all x (the same holds for ϕ_P). Satisfying the second condition when using flows corresponds to proving that every point in X flows into Y in *finite* time. Finally, the third condition of Proposition 3.1 requires the set Y to be *flow-tight* under the applied flow map, meaning that no point of Y flows out of it and therefore $\phi_S(Y) = Y$.

Crucial to our homotopy equivalence proofs is the concept of reduced shapes.

3.1 Reduced Shapes

Reduced Shapes Let S be a shape whose boundary is a smooth 2-manifold Σ and let $0 < \delta < 1$. The *δ-tubular neighborhood* Σ_δ of Σ (See Figure 3) is the set

$$\Sigma_\delta = \Sigma \cup \{x \in \mathbb{R}^3 \setminus (\Sigma \cup M) \,:\, \|x - \hat{x}\| < \delta f(\hat{x})\}.$$

and the *δ-reduced shape* S_δ is defined as $S_\delta = S \setminus \Sigma_\delta$. Notice that the definition of Σ_δ, puts the medial axis $M(S)$ of S into S_δ. The following lemma shows that every point of $M(S)$ is in fact an interior point of S_δ.

Lemma 3.2 *For every $0 < \delta < 1$, every point of $M(S)$ is an interior point of S_δ.*

Proof. Take $x \in M(S)$ and let $B = B(x,\omega)$ where $\omega = \frac{1-\delta}{1+2\delta} h_S(x) > 0$. We will show that $B \subset S_\delta$ implying that x is an interior point of S_δ. Take any point $y \in B$. If $y \in M(S)$, then $y \in S_\delta$ by definition. Thus assume that $y \notin M(S)$ and therefore has a unique closest point $\hat{y}$ in Σ. Notice that since $B' = B(x, h_S(x)) \subset S$ but $\partial B'$ intersects Σ, we get

$$h_S(x) - \omega \leq h_S(y) \leq h_S(x) + \omega. \tag{3}$$

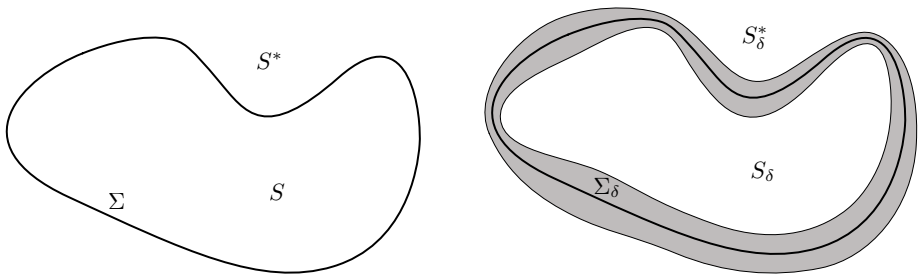

Figure 3: Left: surface Σ and the associated bounded and unbounded shapes S and S^*. Right: the δ-tubular neighborhood Σ_δ (grayed) and the reduced shapes S_δ and S^*_δ.

Moreover, since $x \in M(S)$, we get

$$f(\hat{y}) \leq h_S(y) + \|x - y\| \leq h_S(y) + \omega \leq 2\omega + h_S(x). \tag{4}$$

Combining Equations (3) and (4) and using the definition of ω we obtain

$$h_S(y) \geq h_S(x) - \omega = \delta h_S(x) + 2\delta\omega \geq \delta f(\hat{y}).$$

■

Note, that the previous lemma also implies that every boundary point of S_δ has a unique closest point in Σ. The following lemma gives a complete characterization of the boundary points of S_δ.

Lemma 3.3 *The boundary of S_δ consists of exactly those points $x \in S \setminus M(S)$ satisfying $\|x - \hat{x}\| = \delta f(\hat{x})$.*

Proof. Lemma 3.2 shows that no point of $M(S)$ can be a boundary point for S_δ. For every other point $x \in S$, there is a unique $\hat{x} \in \Sigma$. Consider the segment $\hat{x}\check{x}$. For every point in this segment the closest point in Σ is the same, i.e., $\hat{x}$. Thus, all points in the relative interior of the segment $\hat{x}x$ lie in Σ_δ and all points of the relative interior of $x\check{x}$ lie in S_δ. This implies that x is a boundary point for S_δ.

We now show that S_δ has no other boundary points. First we show that no point $x \in S_\delta \setminus M(S)$ with $h_S(x) = \lambda f(\hat{x})$ where $\lambda > \delta$ can be a boundary point of S_δ. Let $B = B(\check{x}, \mu f(\hat{x}))$ be the medial ball tangent to Σ at $\hat{x}$ at the same side of Σ as x.

To this end, we show that the open ball centered at x and with radius

$$\omega = \frac{(\mu - \lambda)(\lambda - \delta)}{\mu - \lambda + 2\mu\delta} f(\hat{x}) > 0$$

is entirely contained in S_δ. By definition $B \subset S$. Let y be a point at distance less than ω from x. The angle $\alpha = \angle(x - \check{x}, y - \check{x})$ grows when y moves away from x in the direction of $y - x$. When $\|x - y\|$ is fixed, α is maximized when $\angle(\check{x} - y, x - y) = \pi/2$ in which case $\sin\alpha = \omega/((\mu - \lambda)f(\hat{x}))$. The point $\hat{y}$ can be at most as far away from y as $\hat{x}$ is. Therefore, $\hat{y}$ lies in the ball $B' = B(y, \|\hat{x} - y\|)$. Since B is an empty ball, this implies that the distance between $\hat{y}$ and $\hat{x}$ is at most $2\mu f(\hat{x}) \sin\alpha = 2\mu\omega/(\mu - \lambda)$ and from that we get

$$f(\hat{y}) \leq f(\hat{x}) + \|\hat{x} - \hat{y}\| \leq f(\hat{x}) + \frac{2\mu\omega}{\mu - \lambda}.$$

On the other hand,

$$h_S(y) \geq h_S(x) - \omega = \lambda f(\hat{x}) - \omega \geq \delta \left(f(\hat{x}) + \frac{2\mu\omega}{\mu - \delta} \right) \geq \delta f(\hat{y}).$$

Since y was taken arbitrarily from $B(x, \omega)$, it follows that $B(x, \omega) \subset S_\delta$, meaning x is an interior point of S_δ.

Finally we show that no point of Σ_δ can be a boundary point of S_δ. Let $x \in \Sigma_\delta$ be a point for which $h_S(x) = \lambda f(\hat{x})$ where $\lambda < \delta$. Let μ be as above. Consider the open ball of radius $\omega = \frac{(\delta-\lambda)(\mu-\lambda)}{\mu-\lambda+2\mu\delta} f(\hat{x}) > 0$ and let y be a point in this ball. Similar to the previous case, we can show that $\|\hat{y} - \hat{x}\| \leq 2\mu\omega/(\mu - \lambda)$ and therefore

$$f(\hat{y}) \geq f(\hat{x}) - \frac{2\mu\omega}{\mu - \lambda}.$$

On the other hand $h_S(y) < h_S(x) + \omega$. Combining these we get

$$h_S(y) < h_S(x) + \omega = \lambda f(\hat{x}) + \omega \leq \delta \left(f(\hat{x}) - \frac{2\omega}{\mu - \lambda} \right) < \delta f(\hat{y}).$$

■

3.2 Homotopy Proofs

Our proof that the core $\mathcal{C}$ and the medial axis $M(S)$ of S are homotopy equivalent consists of the following two steps.

(1) S and S_δ are homotopy equivalent for $0 < \delta < 1$.

(2) $S_{2\varepsilon^2}$ and $\mathcal{C}$ are homotopy equivalent for $\varepsilon < 0.14$.

The equivalences (1) and (2) together with the homotopy equivalence of S and $M(S)$ [16] establish the homotopy equivalence of $M(S)$ and $\mathcal{C}$.

As we mentioned earlier an essential part of each of the homotopy equivalence proofs consists of showing, in correspondence to the second condition of Proposition 3.1, that a considered object is flow-tight under some flow. Trivially, every open set S is flow-tight with respect to the flow ϕ_S it induces. The medial axis $M(S)$ of an open set S is also flow-tight under ϕ_S. This is because $M(S)$ precisely consists of the points $x \in S$ for which $|A_S(x)| > 1$ and consequently $r_S(x) > 0$. This observation, along with a result of Lieutier [16] that states that the map $t \mapsto r_S(\phi_S(t, x))$ is increasing for every $x \in S$, implies that the flow orbit of every point $x \in M(S)$ stays inside $M(S)$.

Proposition 3.4 *The medial axis $M(S)$ of any open set S is flow-tight under the flow ϕ_S.*

The following lemma, due to Lieutier [16], shows that every point $x \in S$ arrives in $M(S)$ under ϕ_S in finite time. We reproduce the proof of the Lemma for the sake of completeness and because it is a good example for demonstrating the technique we employ in homotopy equivalence proofs in the sequel.

Lemma 3.5 [16] *Let Δ be an upper bound for the diameter of an open set S. Then for every $x \in S$, we have $\phi_S(\Delta, x) \in M(S)$.*

Proof. By Proposition 3.4, if $\phi_S(\Delta, x) \notin M(S)$, it must be that $\phi_S(t, x) \notin M(S)$ for all $t \in [0, \Delta]$. Since for every point x outside the medial axis $r_S(x) = 0$ and therefore by Eq. (1) $\|v_S(x)\| = 1$, if $\phi_S(\Delta, x) \notin M(S)$ by Eq. (2) we get

$$\begin{aligned} h_S(\phi_S(\Delta, x)) &= h_S(x) + \int_0^\Delta \|v_S(\phi_S(\tau, x))\|^2 d\tau \\ &\geq h_S(x) + \int_0^\Delta d\tau = h_S(x) + \Delta. \end{aligned}$$

However, $h_S(x) < \Delta$ for every point $x \in S$, a contradiction. ■

The above lemma together with Proposition 3.4 and the fact that $\phi_S(0, x) = x$ for all $x \in S$ shows that ϕ_S fulfills the three conditions of Proposition 3.1 and therefore implies the following result of Lieutier [16].

Corollary 3.6 [16] *Every bounded open subset S of $\mathbb{R}^3$ is homotopy equivalent to its medial axis $M(S)$.*

Next we show that the reduced shapes S_δ for $0 < \delta < 1$ are also flow-tight under the flow ϕ_S. By Proposition 3.1 this implies that S and S_δ are homotopy equivalent for $0 < \delta < 1$.

Lemma 3.7 *For any $0 < \delta < 1$, the reduced shape S_δ is flow-tight under the flow ϕ_S.*

Proof. By Lemma 3.3, the boundary points of S_δ are exactly those x satisfying $h_S(x) = \delta f(\hat{x})$. The flow vector $v_S(x)$ for any such point is exactly $(x - \hat{x})/h(x)$ which is a unit vector in the direction of normal to Σ at $\hat{x}$. In fact, the flow direction remains constant on the relative interior of the segment $\hat{x}\check{x}$. For every such point y, $\hat{y} = \hat{x}$ and therefore $f(\hat{y}) = f(\hat{x})$ remains the same while the distance to $\hat{x}$ grows larger than $\delta f(\hat{x})$ as soon as the flow passes through x. Thus, the flow direction at every boundary point of S_δ points toward the interior of S_δ. ■

Corollary 3.8 *For any $0 < \delta < 1$, any bounded open set S is homotopy equivalent to its δ-reduced shape S_δ.*

To complete the proof of homotopy equivalence between S and $\mathcal{C}$ we now integrate the vector field v_P (induced by the sample P) to get a flow map ϕ_P and show that the reduced shape S_δ is also flow-tight under the flow ϕ_P for some range of suitable values of δ. However, in doing so, we face a technical difficulty. The results of Lieutier [16] on existence and continuity of the flow map only apply when the set of points that induces the map is *bounded* and open. Although P^c is open, it is not bounded. A standard technique lets us bypass this problem. Let $B_0 = B(c, \Delta/2)$ be an open ball of center c and diameter Δ such that $S \subset B_0$ and thus Δ is an upper bound for diameter of S and let $B_1 = 3B_0 = B(c, 3\Delta/2)$ be the result of scaling B_0 three times around its center. Finally let Q be the open set obtained by removing the sample points in P from B_1, i.e., $Q = B_1 \setminus P$. Notice that $\partial Q = P \cup \partial B_1$. For any point x in S, the closest boundary point of Q to x is a point of P. This is because every boundary point of B_1 is at distance strictly greater than Δ or more from x while there is always a point of P within distance strictly less than Δ from x. This in particular means that the flow induced by Q in S, entirely depends on the arrangement of the points in P only and is completely irrelevant to the boundary of B_1. In other words, the flow lines of the flow ϕ_Q agree with those of the discrete flow ϕ_P inside S as described by [12]. As such, in the sequel we shall use the notation ϕ_P to denote the *continuous* flow induced by the open set Q inside B_0. In order to prove an analogue of Lemma 3.7 for the flow ϕ_P, we first prove following two auxiliary lemmas. The proofs of these lemmas are primarily based on the Lipschitzness of the local feature size function.

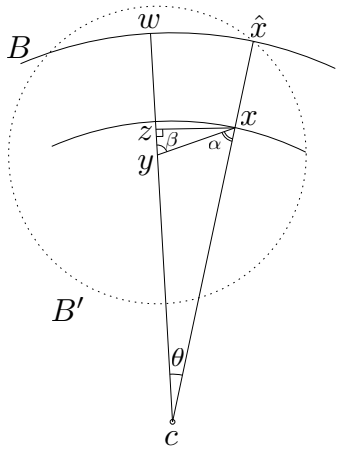

Figure 4: Proof of Lemma 3.9.

Lemma 3.9 *Let x be a point on the boundary of S_δ. Any vector v at x that makes an angle α less than*

$$\arctan\left(\frac{1-\delta}{2\delta}\right)$$

with the vector $\check{x} - x$ points into S_δ.

Proof. Let c be the point on the line segment $\hat{x}\check{x}$ at distance $f(\hat{x})$ from $\hat{x}$. Without loss of generality we assume that $v = y - x$, where $y \in S$ is chosen close enough to x such that the inner angle θ of the triangle xcy at c is less than $\pi/2 - \alpha$. Note that by definition α is the inner angle of the triangle xcy at x, see Figure 4. Let $B = B(c, f(\hat{x}))$ and let $B' = \overline{B}(y, \|\hat{x} - y\|)$. B does not contain any point from Σ and $\hat{y} \in B'$. Therefore $\hat{y} \in B' \setminus B$ and $\|\hat{x} - \hat{y}\| \leq 2f(\hat{x}) \sin\theta$, which in turn together with the fact that f is 1-Lipschitz implies that

$$f(\hat{y}) \leq f(\hat{x})(1 + 2\sin\theta).$$

Let w be the intersection point of the boundary of B with the ray through $y - c$ and let z be the projection of x on this ray. By construction $z \in B$. Our assumption on θ implies that on the ray through $c - y$ the point y comes before the point z as seen from c. Putting everything together we get

$$\begin{aligned}
\|y - \hat{y}\| &\geq \|y - w\| \\
&= \|y - z\| + \|z - w\| \\
&> \|y - z\| + \|x - \hat{x}\| \\
&= \|y - z\| + \delta f(\hat{x}) \\
&= \|x - z\| \cot(\alpha + \theta) + \delta f(\hat{x}) \\
&= (1 - \delta) f(\hat{x}) \sin\theta \cot(\alpha + \theta) + \delta f(\hat{x}).
\end{aligned}$$

Thus,

$$\begin{aligned}
\frac{\|y - \hat{y}\|}{f(\hat{y})} &> \frac{(1-\delta) f(\hat{x}) \sin\theta \cot(\alpha + \theta) + \delta f(\hat{x})}{f(\hat{x})(1 + 2\sin\theta)} \\
&= \frac{(1-\delta)\sin\theta \cot(\alpha + \theta) + \delta}{1 + 2\sin\theta}.
\end{aligned}$$

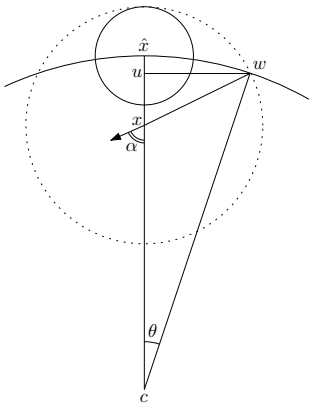

Figure 5: Proof of Lemma 3.10.

In order for y to be in S_δ we want this fraction to be larger than δ. This amounts to $\cot(\alpha+\theta) > 2\delta/(1-\delta)$ or equivalently $\tan(\alpha+\theta) < (1-\delta)/2\delta$. Since we assumed $\tan\alpha < (1-\delta)/2\delta$ we can find by the continuity of the tangent function $\theta_0 > 0$ such that $\tan(\alpha+\theta) < (1-\delta)/(2\delta)$ for all $0 < \theta < \theta_0$. This implies the existence of $\lambda_0 > 0$ such that

$$(1-\lambda)x + \lambda y = x + \lambda(y-x) = x + \lambda v \in S_\delta$$

for all $0 \leq \lambda < \lambda_0$, i.e., the vector v points into S_δ at x. ■

Lemma 3.10 *Let x be a point on the boundary of S_δ. The angle α that $v_P(x)$ makes with $\check{x} - x$ is bounded by*

$$\arccos\left(\frac{2\delta(1-\varepsilon-\delta)-\varepsilon^2}{2(1-\delta)(\delta+\varepsilon)}\right),$$

provided that the argument of the arccos *is between* 0 *and* 1.

Proof. Let c be the point on the line segment $\hat{x}\check{x}$ at distance $f(\hat{x})$ from $\hat{x}$. Let $B = B(c, f(\hat{x}))$ and let $B' = \overline{B}(x, (\delta+\varepsilon)f(\hat{x}))$. The driver $d_P(x)$ of x has to be contained in the convex hull of $B' \setminus B$. Let w be a point in the intersection of ∂B and $\partial B'$. Consider the triangle cxw, see Figure 5. The inner angle of this triangle at x is at least $\pi - \alpha$. From the cosine theorem we get

$$\begin{aligned}\cos(\pi-\alpha) &\leq \frac{(1-\delta)^2 f(\hat{x})^2 + (\delta+\varepsilon)^2 f(\hat{x})^2 - f(\hat{x})^2}{2(1-\delta)(\delta+\varepsilon)f(\hat{x})^2} \\ &= \frac{2\delta(\delta+\varepsilon-1)+\varepsilon^2}{2(1-\delta)(\delta+\varepsilon)}.\end{aligned}$$

It follows

$$\cos\alpha \geq \frac{2\delta(1-\delta-\varepsilon)-\varepsilon^2}{2(1-\delta)(\delta+\varepsilon)},$$

which implies the statement of the lemma. ■

Now we are ready to prove the analogue of Lemma 3.7 for the flow ϕ_P.

Lemma 3.11 *The δ-reduced shape S_δ is flow-tight under the flow ϕ_P, respectively, for any $\varepsilon^2 \leq \delta \leq 10\varepsilon^2$ if $\varepsilon \leq 0.14$.*

Proof. Using Lemmas 3.9 and 3.10 if parameters ε and δ are chosen in a way that

$$\arccos\left(\frac{2\delta(1-\varepsilon-\delta)-\varepsilon^2}{2(1-\delta)(\delta+\varepsilon)}\right) \leq \arctan\left(\frac{1-\delta}{2\delta}\right),$$

then at any point x on the boundary of S_δ, the vector $v_P(x)$ points into S_δ. It can be verified that for $\varepsilon \leq 0.14$, the above inequality is satisfied when δ falls in the interval $[\varepsilon^2, 10\varepsilon^2]$. ■

Lemma 3.11 now allows us to prove that the core $\mathcal{C}$ and S_δ are homotopy equivalent. To do so we need the following corollary and lemma.

Corollary 3.12 *For any $\varepsilon^2 \leq \delta < 10\varepsilon^2$ and $\varepsilon \leq 0.14$, every point of the reduced shape S_δ flows under ϕ_P into an inner medial axis critical point of h_P.*

Proof. By Lemma 3.11 every point of S_{ε^2} stays inside S_{ε^2} under ϕ_P while all surface critical points of h_P are in Σ_{ε^2} by Theorem 2.1. Since P is a finite point set and therefore all flow orbits converge to critical points, the flow orbit $\phi_P(x)$ of every point $x \in S_\delta \subseteq S_{\varepsilon^2}$ has to end at a critical point contained in S_{ε^2}, i.e. an inner medial axis critical point. ■

Lemma 3.13 *If $\varepsilon \leq 0.14$ and $\varepsilon^2 \leq \delta \leq 10\varepsilon^2$ then $\mathcal{C} \subset S_\delta$.*

Proof. By Theorem 2.1, the inner medial axis critical points of h_P are contained in $S_{1-2\varepsilon^2} \subset S_\delta$. In fact, $1-2\varepsilon^2 > 10\varepsilon^2$ implies that for every inner medial axis critical point c, some neighborhood of c is contained in S_δ in addition to c. Every point of $x \in \mathcal{C}$ is on the flow orbit $\phi_P(y)$ of a point y infinitesimally close to some inner medial axis critical point c and is therefore in S_δ. On the other hand, by Lemma 3.11, S_δ is flow-tight for our choices ε and δ. Thus x being on the orbit of a point $y \in S_\delta$ has to be in S_δ as well. ■

Lemma 3.14 *For $\varepsilon \leq 0.14$, if P is an ε-sample of Σ, then there is a constant T such that $\phi_P(T, x) \in \mathcal{C}$ for all $x \in S_{2\varepsilon^2}$.*

Proof. Let $\zeta > 0$ be the minimum distance between a Delaunay face D in the Delaunay complex $\mathrm{Del}(P)$ of P and its dual Voronoi face V that do not intersect. Consider the reduced set S_δ for $\delta = 2\varepsilon^2$. By Corollary 3.12, S_δ is flow-tight under the flow ϕ_P. Therefore, every flow line of ϕ_P in S_δ ends in some inner medial axis critical point of h_P in the limit. Consider now any point $x \in S_\delta \setminus \mathcal{C}$ and let $V(x)$ be the cell in the Voronoi complex $\mathrm{Vor}(P)$ that contains x and let $D(x)$ be its dual Delaunay cell in the Delaunay complex $\mathrm{Del}(P)$. There are two cases to consider depending on whether $V(x)$ and $D(x)$ intersect.
Case 1. $V(x) \cap D(x) = \emptyset$. In this case, the distance $\|x - d_P(x)\| \geq \zeta$ and since $h_P(x) \leq \Delta$, we get

$$\|v_P(x)\| = \|x - d_P(x)\|/h_P(x) \geq \zeta/\Delta.$$

Case 2. $V(x) \cap D(x) = \{c\}$, where c is a critical point of h_P. It can be easily observed that if c is a medial axis critical point, then $V(x)$ is entirely contained in the unstable manifold $\mathrm{Um}(c)$ of c and this implies that $x \in \mathcal{C}$, contradicting our choice of x. Therefore, c must be a surface critical point and therefore $c \in \Sigma_{\varepsilon^2}$ while $x \in S_{2\varepsilon^2}$. With a similar argument to the one used in Lemma 3.3, if we use $\delta = 2\varepsilon^2$ and $\lambda = \varepsilon^2$, the open ball with center c and radius $\frac{(\delta-\lambda)(1-\lambda)}{1-\lambda+2\delta} f(\hat{c})$ is entirely contained in $\Sigma_{2\varepsilon^2}$ and therefore $\|x - c\| \geq \xi := \frac{(1-\varepsilon^2)\varepsilon^2}{1+3\varepsilon^2} f_0$. Thus we get

$$\|v_P(x)\| = \|x - c\|/h_P(x) \geq \xi/\Delta.$$

Thus for every point $x \in S_\delta \setminus \mathcal{C}$, $\|v_P(x)\| \geq \vartheta$ where $\vartheta := \min\{\xi/\Delta, \zeta/\Delta\}$. If $\phi_P(t,x) \notin \mathcal{C}$ for all $t \in [0, \Delta/\vartheta^2]$ we get from Eq. (2)

$$\begin{aligned} h_P(\phi_P(\Delta/\vartheta^2, x)) &= h_P(x) + \int_0^{\frac{\Delta}{\vartheta^2}} \|v_P(\phi_P(\tau, x))\|^2 d\tau \\ &\geq h_P(x) + \int_0^{\frac{\Delta}{\vartheta^2}} \vartheta^2 d\tau = h_P(x) + \Delta. \end{aligned}$$

This contradicts the fact that Δ is an upper bound for the diameter of S. Thus if we set $T = \Delta/\vartheta^2$, then $\phi_P(T, x) \in \mathcal{C}$ for all $x \in S_\delta \setminus \mathcal{C}$. ■

Corollary 3.15 *For $\varepsilon \leq 0.14$, if P is an ε-sample of Σ, then $\mathcal{C}$ is homotopy equivalent to $S_{2\varepsilon^2}$.*

Proof. By definition, $\mathcal{C}$ is flow-tight under the flow ϕ_P. This along with the result of Lemma 3.13 and Lemma 3.14 shows that ϕ_P satisfies the conditions of Proposition 3.1, implying that $\mathcal{C}$ and $S_{2\varepsilon^2}$ are homotopy equivalent. ■

Combining the result of the above corollary with that of Corollary 3.8 gives us the theorem we set out to prove.

Theorem 3.16 *The shape S, its medial axis $M(S)$, and the core $\mathcal{C}$ consisting of the the union of unstable manifolds of inner medial axis critical points of h_P, are homotopy equivalent.*

3.3 Extending the Core

As mentioned in the Introduction section, an interesting property of the core is its flexibility when being used with other medial axis approximation algorithms. The following theorem clarifies this statement.

Theorem 3.17 *Let $W \subset S_{2\varepsilon^2}$ be any set of points and let $\widehat{W} = \phi_P(W) = \{x \mid \exists w \in W : x \in \phi_P(w)\}$. Then $\mathcal{C} \cup \widehat{W}$ is homotopy equivalent to S.*

Proof. By Lemma 3.14 all points in $S_{2\varepsilon^2}$ including those in $\widehat{W}$ flow into $\mathcal{C}$ in finite time. On the other hand, by definition $\mathcal{C} \cup \widehat{W}$ is flow-tight for ϕ_P. These are all the requirements needed to invoke Proposition 3.4 to establish the desired homotopy equivalence between $\mathcal{C} \cup \widehat{W}$ and $S_{2\varepsilon^2}$. By Corollary 3.8, the latter is itself homotopy equivalent to S. ■

Computing the flow closure of all the points in W can be computationally difficult, depending on the nature of W. However, If W is a sub-complex of the Voronoi complex $\mathrm{Vor}(P)$ (this is for example the case in the algorithm of Dey and Zhao [10]), computing the flow closure of all the points in W can be done in bulk by computing the flow closures of a whole face at a time. An algorithm for computing the flow closure of a Voronoi face can be found in Section 5. Note that this algorithm can also be used for computing the core since the unstable manifold of a critical point is the flow closure of the Voronoi face that contains it.

4 Geometric Approximation

Although Theorem 2.1 ensures that the medial axis critical points lie very close to the medial axis, it provides no guarantee for the closeness of medial axis and the paths connecting medial axis critical points on their unstable manifolds. The same concern is valid when we extend the core

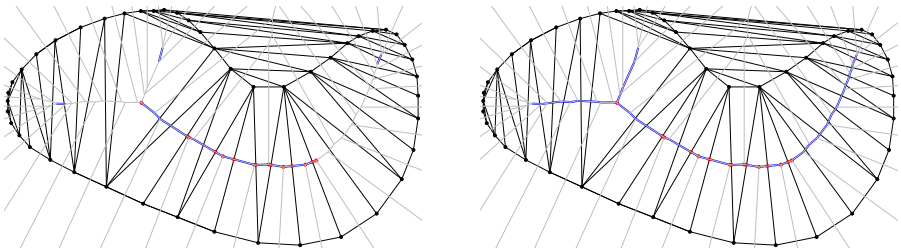

Figure 6: Extending the Core. Left: The core, i.e. the union of unstable manifolds of medial axis critical points of the sampled curve is shown in bold in the middle. The three isolated short segments also shown in bold represent geometrically intersesting parts of the medial axis of shape enclosed by the curve. Right: The flow closure of the three segments are added to the core to result a topologically valid approximation of the medial axis.

with a set of points close the medial axis: to guarantee the topology one must include the flow closures of added points but it is not clear that this closure stays close to the medial axis as well.

For a point x in the core $\mathcal{C}$ or any other approximation of the medial axis, the *relative* approximation error at x can be considered to be the ratio between the distance from x to $M(S)$ and $h_P(x)$. One would like to have that the distance to $M(S)$ along a flow line would grow at most linearly with $h_P(x)$ as this would correspond to maintaining a constant relative error all along the path. However, proving this, if it is true at all, appears elusive. Nevertheless, in this section we show that if we start from a point x close to the medial axis and follow the flow line $\phi_P(x)$, the distance to $M(S)$ along this path grows as a function of h_P at a rate slightly super-linear at worst. More precisely we will show that if we scale the space so that $h_P(x)$ has unit length, then if x has a medial axis point within distance $O(\sqrt{\varepsilon})$, every point y in the flow line starting at x will have a medial axis point within distance $O(\sqrt{\varepsilon})h_P(y)^{1+O(\sqrt{\varepsilon})}$. This is achieved through a sequence of observations stated through the following lemmas.

Lemma 4.1 *For every point $x \in S$ and for every $p \in A_P(x)$, $\|x-p\|^2 \leq h_S(x)^2 + \varepsilon^2 f(\hat{x})^2 + \varepsilon^2 h_S(x) f(\hat{x})$.*

Proof. Let $B = B(\hat{x}, \varepsilon f(\hat{x}))$. By the ε-sampling condition, the closest sample point to $\hat{x}$ is at distance no more than $\varepsilon f(\hat{x})$ from $\hat{x}$. In other words, B must contain at least one point from P.

Let B_i and B_o be two ball of radius $f(\hat{x})$ tangent to Σ at $\hat{x}$, with B_i contained in S and B_o outside of it. Also, let x_i and x_o be the centers of B_i and B_o, respectively. Since B_i and B_o cannot contain any sample points, the closest sample point to $\hat{x}$ must lie in the region $S = B \setminus (B_i \cup B_o)$. It is easy to see that the points in S that are farthest from x are those in $\partial B \cap \partial B_o$. Let y be one such point. $\|x-y\|$ is therefore an upper bound for $h_P(x)$. Consider the plane Π containing x, $\hat{x}$ and y, and consequently $\check{x}$ and x_o, see Figure 7. The intersection of B, B_i and B_o with Π are circles to which we shall refer in Figure 7 with the names of the corresponding balls. Let z and z' be the points where the bisector of $\angle \hat{x} x_o y$ meets the segment $\hat{x}y$ and the bisector of $x_i x_o$, respectively.

The two triangles $x_o \hat{x} z'$ and $z \hat{x} z'$ are similar and therefore $\alpha = \angle z x_o \hat{x} = \angle z \hat{x} z'$. Furthermore, since $\|\hat{x} - y\| = \varepsilon f(\hat{x})$, $\sin \alpha = \varepsilon/2$. We have for the distance of x and y:

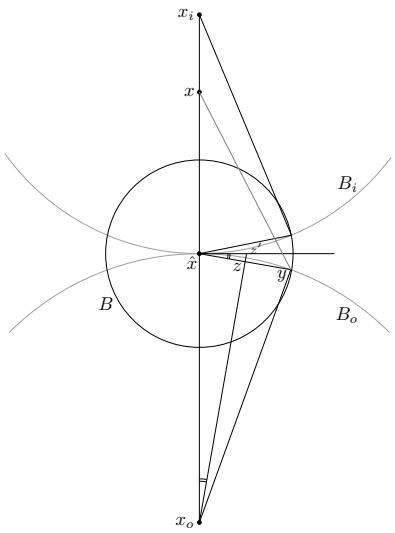

Figure 7: proof of Lemma 4.1

$$\begin{aligned}\|x-y\|^2 &= \|x-\hat{x}\|^2 + \|\hat{x}-y\|^2 - 2\|x-\hat{x}\|\cdot\|\hat{x}-y\|\cos(\pi/2+\alpha)\\ &= h_S(x)^2 + \varepsilon^2 f(\hat{x})^2 + 2\varepsilon h_S(x) f(\hat{x})\sin\alpha\\ &= h_S(x)^2 + \varepsilon^2 f(\hat{x})^2 + \varepsilon^2 h_S(x) f(\hat{x}).\end{aligned}$$

■

The *driving angle* of a point x with respect to the sample P is defined as $\theta_P(x) := \angle(-v_P(x), y-x)$ for any $y \in A_P(x)$. A critical point has driving angle equal to $\pi/2$ while points not on the 2-skeleton of $\mathrm{Vor}(P)$ have driving angles equal to 0. It is not hard to verify that $\cos\theta_P(x) = \|v_P(x)\|$.

The following lemma generalizes Theorem 2.1 although for simplicity it provides a weaker bound for points near the surface. The proof is rather similar to the one given in [9].

Lemma 4.2 *Let x be a point with driving angle $0 < \theta \le \pi/2$. Then, x is within distance $\frac{2\varepsilon}{1-\cos\theta}\mu(x)$ from one of $\hat{x}$ or $\check{x}$.*

Proof. Let $\lambda = \|x-\check{x}\|/\mu(x)$ The ball $B = B(\check{x}, \mu(x))$ contains no sample points. On the other hand, there is a sample point within distance $\varepsilon\mu(x)$ from $\hat{x}$. By triangle inequality, this implies that there is a sample point within distance $(1-\lambda+\varepsilon)\mu(x)$ from x. Consider the ball $B' = B(x, (1-\lambda+\varepsilon)\mu(x))$. All sample points in $A_P(x)$ are contained in $B' \setminus B$. This implies that the angle $\angle(-v(x), y-x)$ is at least θ for any $y \in \partial B' \cap \partial B$. Thus using the cosine rule on the triangle $\check{x}xy$ for any such y, we get the following inequality.

$$\mu(x)^2 \le \lambda^2\mu(x)^2 + (1-\lambda+\varepsilon)^2\mu(x)^2 + 2\lambda\mu(x)(1-\lambda+\varepsilon)\mu(x)\cos\theta,$$

or equivalently

$$2(1-\cos\theta)\lambda^2 - 2(1+\varepsilon)(1-\cos\theta)\lambda + \varepsilon(2+\varepsilon) \ge 0.$$

Solving this inequality for λ we conclude that either,

$$\begin{aligned}
\lambda &\leq \frac{1+\varepsilon}{2}\left(1-\sqrt{1-\frac{2\varepsilon(2+\varepsilon)}{(1-\cos\theta)(1+\varepsilon)^2}}\right)\\
&\leq \frac{1+\varepsilon}{2}\cdot\frac{2\varepsilon(2+\varepsilon)}{(1-\cos\theta)(1+\varepsilon)^2}\\
&\leq \frac{2\varepsilon}{1-\cos\theta},
\end{aligned}$$

or

$$\begin{aligned}
\lambda &\geq \frac{1+\varepsilon}{2}\left(1+\sqrt{1-\frac{2\varepsilon(2+\varepsilon)}{(1-\cos\theta)(1+\varepsilon)^2}}\right)\\
&\geq \frac{1+\varepsilon}{2}\left(2-\frac{2\varepsilon(2+\varepsilon)}{(1-\cos\theta)(1+\varepsilon)^2}\right)\\
&\geq 1+\varepsilon-\frac{\varepsilon(2+\varepsilon)}{(1-\cos\theta)(1+\varepsilon)}\\
&\geq 1-\frac{2\varepsilon}{1-\cos\theta},
\end{aligned}$$

■

Remark. A slicker analysis as the one used in the proof of the separation of critical points in [9] can result tighter bounds for λ.

Recall that the driver $d_P(x)$ is the same for all points x of the relative interior of the same Voronoi face in $\mathrm{Vor}(P)$. In fact the flow orbit $\phi_P(t,x)$ turns exactly when the flow moves from one Voronoi face to another. Consider a point $x \in S$ that lies on the 2-skeleton of $\mathrm{Vor}(P)$, i.e., $|A_P(x)| \geq 2$, and consider a line segment L in the flow orbit $\phi_P(t,x)$. The distance $h_P(x)$ monotonically increases along a flow orbit. We can therefore parametrize this line segment using the distance to the sample set P. Let $g : \mathbb{R}^+ \to \mathbb{R}^+$ be a non-decreasing real valued differentiable function and consider for each point $y \in L$, the ball $B_g(y) = B(y, g(h_P(y)))$. We define the set $D(y)$ as those points on the boundary of $B_g(y)$ that are left outside $B_g(y)$ when y moves infinitesimally in the direction of $\phi_P(t,y)$. In other words if we take $\eta > 0$ such that $\phi_P(\eta, y)$ has the same driver as $d_P(y)$ (meaning that $\phi_P(\eta,y)$ is on the same line segment of $\phi_P(t,x)$ as y), then

$$D(y) = \bigcap_{0<\lambda<\eta} \left(\partial B_g(y) \setminus \overline{B}_g(\phi_P(\lambda, y))\right).$$

Lemma 4.3 *$D(x)$ consists of those points $y \in \partial B_g(x)$ that satisfy $\angle(y-x, d_P(x)-x) \leq \psi_0$ where $\cos\psi_0 = dg/dh_P$ at x.*

Proof. Let $x' = \phi_P(t,x)$ be a point on L, satisfying $\|x-x'\| = \tau$ where τ is infinitesimally small. By definition, $A_P(x') = A_P(x)$. Let y be any point at distance $g(h_P(x))$ from x making an angle of ψ with $d_P(x) - x$. We have for the distance of y to x':

$$\begin{aligned}
\|y-x'\|^2 &= \|y-x\|^2 + \tau^2 + 2\tau\|x-y\|\cos\psi\\
&= g(h_P(x))^2 + \tau^2 + 2\tau g(h_P(x))\cos\psi.
\end{aligned}$$

For y not to be contained in $B_g(x')$ it must hold that $\|y-x'\| > g(h_P(x'))$, or equivalently:

$$g(h_P(x))^2 + \tau^2 + 2\tau g(h_P(x))\cos\psi > g(h_P(x'))^2.$$

By rearranging we get

$$\tau + 2g(h_P(x))\cos\psi > \frac{g(h_P(x)+\tau)^2 - g(h_P(x))^2}{\tau}.$$

In the limit $\tau \to 0$ we get

$$\lim_{\tau\to 0} \tau + 2g(h_P(x))\cos\psi \geq \lim_{\tau\to 0} \frac{g(h_P(x)+\tau)^2 - g(h_P(x))^2}{\tau},$$

which gives

$$\begin{aligned} 2g(h_P(x))\cos\psi &\geq \frac{d}{dh_P}\left(g(h_P(x))\right)^2 \\ &= 2g(h_P(x))\frac{d}{dh_P}g(h_P(x)). \end{aligned}$$

Thus $\cos\psi \geq \cos\psi_0$ or $\psi \leq \psi_0$. ■

Lemma 4.4 *Let $B = B(x,R)$ be a ball empty of sample points with at least one sample point on its boundary and containing at least one medial axis point. Then the ball $B(x,(1-4\varepsilon^2)R)$ does not intersect Σ.*

Proof. Let z be a point in $B \cap \Sigma$. Since B intersects the medial axis, $f(z) \leq 2R$. Thus there is a sample point within distance $\varepsilon f(z) \leq 2\varepsilon R$ from z. Since B contains no sample points, z must be within distance $2\varepsilon R$ from ∂B. We grow a ball B' centered at x until its boundary touches Σ. Let R' be the radius of B'. By the above argument $R' \geq (1-2\varepsilon)R$. Let y be a point in which B' touches Σ. Similar to the case of z above, $f(y) \leq 2R$. Let B_o be the tangent ball of radius $f(y)$ at the opposite side of Σ with respect to x. With an argument similar to that of Lemma 4.1 we get for $h_S(x) = \|x-y\|$,

$$R^2 \leq h_S(x)^2 + \varepsilon^2 f(y)^2 + \varepsilon^2 h_S(x) f(y).$$

Using $f(y) \leq 2R$ we get

$$R^2 \leq h_S(x)^2 + 4\varepsilon^2 R^2 + 2\varepsilon^2 R h_S(x),$$

which by rearranging gives the following quadratic inequality for $h_S(x)$:

$$h_S(x)^2 + 2\varepsilon^2 R h_S(x) - (1-4\varepsilon^2)R^2 \geq 0.$$

Since $h_S(x) \geq (1-2\varepsilon)R$, the only valid range for $h_S(x)$ in the above inequality is

$$h_S(x) \geq \varepsilon^2 R^2 + \sqrt{\varepsilon^4 R^2 + (1-4\varepsilon^2)R^2} \geq (1-4\varepsilon^2)R.$$

■

Theorem 4.5 *Let $x_0 \in S$ be a point with $|A_P(x_0)| \geq 2$ and $h_P(x_0) = h_0$, and let $x_1 = \phi_P(t_1, x_0)$ be such that for all $0 \leq t \leq t_1$, $\cos(\theta_P(\phi_P(t,x_0))) \geq c$. If there is a medial axis point within distance g_0 from x_0, then there is a medial axis point within distance $g(x_1) = g_0(h_P(x_1)/h_P(x_0))^\xi$ from x_1, provided that $\xi \geq \frac{1}{c}(1 + 4\varepsilon^2 h_0^2/g_0^2)$ and*

$$h_P(x_1) \leq h_0 \cdot \left((1-4\varepsilon^2)\cdot\frac{h_0}{g_0}\right)^{\frac{1}{\xi-1}}.$$

Proof. We prove the theorem by showing that as x moves along the flow line, there always remains a medial axis point within distance $g_0(h_P(x)/h_P(x_0))^\xi$ from x. We do this by showing that this proposition is maintained when x moves infinitesimally along the flow line. To this end, we first recall that the ball $B_g(x)$ is an open ball by definition. If $B_g(x)$ contains a medial axis point z, then for any direction vector v, there is a small enough real number $\tau > 0$, such that the translated ball $B_g(x) + \tau v = \{y + \tau v \mid y \in B_g(x)\}$ contains z as well. Since g is increasing, this implies that $z \in B_g(x + \tau v)$. In particular this implies by choosing $v = v_P(x)$ that if $B_g(x)$ contains a medial axis point, so does $B_g(x + \tau v_P(x))$ for τ sufficiently small.

We thus only need to consider the case where $B_g(x)$ contains no medial axis point while its boundary does. Thus, let $z \in \partial B_g(x)$ be a medial axis point. By Lemma 4.3, if $\cos(\angle(z - x, -v_P(x))) \leq \frac{d}{dh_P} g(h_P(x))$, then z is contained in $B_g(x + \tau v_P(x))$ for a sufficiently small $\tau > 0$ and therefore we have nothing to prove. Thus we only need to consider the case when

$$\begin{aligned} \cos(\angle(z - x, -v_P(x))) &> \frac{d}{dh_P}(g(h_P(x)) \\ &= \frac{\xi g_0}{h_P(x_0)} \left(\frac{h_P(x)}{h_P(x_0)}\right)^{\xi - 1}. \end{aligned}$$

We denote this maximum angle by ψ. We show that in this case, the flow vector $v_S(z)$ points to the interior of the ball $B_g(x)$. This implies that the flow $\phi_S(z)$ enters $B_g(x)$ and therefore, as argued before, $B_g(x)$ must contain a medial axis point, contradicting our choice of z.

The ball $B(x, h_P(x))$ contains no sample points but includes z, a medial axis point, and therefore by Lemma 4.4, the ball $B_0 = B(x, (1 - 4\varepsilon^2)h_P(x))$ does not intersect Σ. Consider the plane Π tangent to $\partial B_g(x)$ at z. This plane, intersects the ball B_0 in a disk of radius

$$R_0 \geq \sqrt{((1 - 4\varepsilon^2)h_P(x))^2 - g(h_P(x))^2}.$$

The upper bound assumed for $h_P(x_1)$ in the statement of the Theorem implies that $(1-4\varepsilon^2)h_P(x)^2 \geq h(h_P(x))^2$ and therefore R_0 is a real number. We will show that there are surface points at distance less than R_0 from z, i.e. $h_S(z) < R_0$. It can be easily observed that any such surface point must lie on the side of Π opposite to the one containing $B_g(x)$ and therefore $\mathrm{conv}(A_S(x))$ resides on the side of Π opposite to $B_g(x)$. Since $d_S(x) \in \mathrm{conv}(A_S(x))$, this implies that $v_S(x)$ points to the interior of $B_g(x)$, as desired. So, all left to show is that $h_S(z) < R_0$. To prove this, we show that for at least one of the points $y \in A_P(x)$, $\|z - y\| < R_0$. Since $|A_P(x)| \geq 2$, every plane containing the points x and $d_P(x)$ that does not intersect $A_P(x)$ must contain at least one point of $A_P(x)$ on each side. The maximum distance between z and $A_P(x)$ can therefore occur when $|A_P(x)| = 2$ and z is on the bisector plane of the segment connecting the two points in $A_P(x)$. To find this maximum distance we use a change of coordinates. Denoting the three coordinate directions by u_1, u_2, and u_3, we put the origin at x, the driver $d_P(x)$ on the u_1-axis, the two points p_1, p_2 in $A_P(x)$ on the u_1u_2-plane, and z on the u_1u_3-plane, see Figure 8. We can calculate the coordinates of p_1, p_2, and z as follows:

$$\begin{aligned} p_1 &= (h\cos\theta, h\sin\theta, 0), \\ p_2 &= (h\cos\theta, -h\sin\theta, 0), \\ z &= (g(h)\cos\psi, 0, g(h)\sin\psi), \end{aligned}$$

where by θ we denote the the driving angle $\theta_P(x)$ and by h we denote $h_P(x)$. Thus we get for the distance between z and p_1 (same distance between z and p_2):

$$\begin{aligned} \|z - p_1\|^2 &= (h\cos\theta - g(h)\cos\psi)^2 + (h\sin\theta)^2 + (g(h)\sin\psi)^2 \\ &= h^2 + g(h)^2 - 2hg(h)\cos\theta\cos\psi \end{aligned}$$

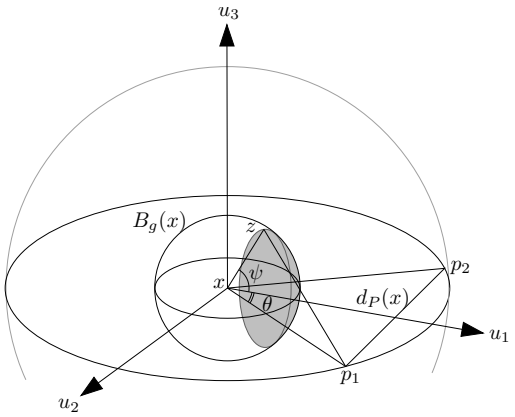

Figure 8: Proof of Theorem 4.5. The gray cap represents $D(x)$.

Denoting $h_P(x_0)$ by h_0 and $h_P(x)$ by h and using the lower bounds for $\cos\psi$ and $\cos\theta$ we get:

$$\begin{aligned}\|z-p_1\|^2 &< h^2+g_0^2\left(\frac{h}{h_0}\right)^{2\xi}-2chg_0\left(\frac{h}{h_0}\right)^{\xi}\frac{\xi g_0}{h_0}\left(\frac{h}{h_0}\right)^{\xi-1}\\ &= h^2+(1-2c\xi)g_0^2\left(\frac{h}{h_0}\right)^{2\xi}\end{aligned}$$

Thus in order for $\|z-p_1\|<R_0$, it suffices to have

$$h^2+(1-2c\xi)g_0^2\left(\frac{h}{h_0}\right)^{2\xi}\leq(1-4\varepsilon^2)^2h^2-g_0^2\left(\frac{h}{h_0}\right)^{2\xi}.$$

Since $(1-4\varepsilon^2)^2>1-8\varepsilon^2$, the above inequality is satisfied when the following one is:

$$4\varepsilon^2h^2\leq(c\xi-1)g_0^2\left(\frac{h}{h_0}\right)^{2\xi},$$

or identically,

$$\frac{4\varepsilon^2}{c\xi-1}\leq\frac{g_0^2}{h_0^2}\left(\frac{h}{h_0}\right)^{2\xi-2}.$$

Since $h/h_0\geq 1$, the above inequality holds if $g_0\geq\left(\frac{2\varepsilon}{\sqrt{c\xi-1}}\right)h_0$. This is guaranteed by the bound on ξ prescribed in the statement of the Theorem. ■

Remark. It may appear at first that when g_0 goes to zero the above theorem must guarantee a tighter bound. However, the reader must notice that g_0 also appears in the denominator of the exponent of the given bound. As a result when the flow line starting at a given x_0 is followed the best bound is not necessarily obtained by using the medial axis point nearest to x_0. In other words, a larger g_0 may lead to a better bound on g.

Corollary 4.6 *For any bounded shape S, there is a small enough ε such that if P is an ε-sample of the boundary of S the following holds: let x be a point in the 2-skeleton of Vor(P) such that $\|x-\check{x}\|\leq\frac{2\sqrt{\varepsilon}}{1-2\sqrt{\varepsilon}}h_P(x)$, then for every point y on the flow path $\phi_P(x)$, there is a medial axis point within distance*

$$\frac{2\sqrt{\varepsilon}}{1-2\sqrt{\varepsilon}}h_P(x)\left(\frac{h_P(y)}{h_P(x)}\right)^{\xi}$$

from y, where $\xi = 1 + \sqrt{\varepsilon} + O(\varepsilon)$.

Proof. We first consider the case where y has a driving angle $\theta = \theta_P(y)$ with $\cos\theta \leq 1 - \sqrt{\varepsilon}$. By Lemma 4.2, $\|y - \check{y}\| \leq 2\sqrt{\varepsilon}\mu(y)$, or equivalently, $h_S(y) \geq (1 - 2\sqrt{\varepsilon})\mu(y)$. Since $h_P(y) \geq h_S(y)$, we get

$$\|y - \check{y}\| \leq 2\sqrt{\varepsilon}\mu(y) \leq \frac{2\sqrt{\varepsilon}}{1 - 2\sqrt{\varepsilon}} h_S(y) \leq \frac{2\sqrt{\varepsilon}}{1 - 2\sqrt{\varepsilon}} h_P(y).$$

Thus we can assume that cosine of the medial angle equals $1 - \sqrt{\varepsilon}$ at x and stays larger than this quantity between x and y. Now, by Theorem 4.5 there always is a point within distance

$$\frac{2\sqrt{\varepsilon}}{1 - 2\sqrt{\varepsilon}} h_P(x) \left(\frac{h_P(y)}{h_P(x)}\right)^{\xi},$$

from y, where

$$\xi = \frac{1}{1 - \sqrt{\varepsilon}} \left(1 + 4\varepsilon^2 \frac{(1 - 2\sqrt{\varepsilon})^2}{(2\sqrt{\varepsilon})^2}\right) \leq 1 + \sqrt{\varepsilon} + O(\varepsilon),$$

so long as

$$h_P(y) \leq h_P(x) \left((1 - 4\varepsilon^2) \cdot \frac{h_P(x)}{\|x - \check{x}\|}\right)^{\frac{1}{\xi - 1}},$$

as required by Theorem 4.5. Since $h_P(x)/\|x - \check{x}\| \geq (1 - 2\sqrt{\varepsilon})/2\sqrt{\varepsilon}$, it is enough to require that

$$\frac{h_P(y)}{h_P(x)} \leq \left((1 - 4\varepsilon^2) \cdot \frac{1 - 2\sqrt{\varepsilon}}{2\sqrt{\varepsilon}}\right)^{\frac{1}{\xi - 1}}.$$

As a function of ε, the right hand side of the above inequality increases when ε decreases. Since S is bounded so is $h_P(y)/h_P(x)$ and therefore for sufficiently small ϵ the statement of this Corollary holds. ■

An immediate consequence of this corollary is that the core and the flow closures converge to being contained in the medial axis as $\varepsilon \to 0$. As a result, when the core is used and extended using the filtering conditions of [10], the computed approximate medial axis converges to the true medial axis in the limit.

5 Algorithms

For our application—medial axis approximation—we need to compute the core, a subset of the of the unstable flow complex, from a finite sampling P of a smooth surface Σ. Our algorithm to compute the unstable flow complex and the unstable manifolds of critical points of h_P that we present in this section are based on an algorithm to compute flow orbits of points under the flow ϕ_P for a finite point set $P \subset \mathbb{R}^3$. We also present a data structure for the unstable flow complex—a directed acyclic graph, that essentially describes a subdivision of Voronoi facets.

To devise an algorithm that computes the flow orbits we use the oracle DRIVER(x) that gives us for any query point $x \in \mathbb{R}^3$ its driver. The oracle basically has to solve the point location problem in the Voronoi diagram of the sample points P to find the lowest dimensional Voronoi face that contains x and then compute the closest point on the Delaunay face dual to this Voronoi face. The oracle returns a tuple (d, V), where d is the driver of x and V is the Voronoi face dual to the lowest dimensional Delaunay face that contains d. Note that d is the driver of all points in the relative interior of V and it is also the driver of x, which can be in the boundary of V. The algorithm in Figure 9 computes the orbit of a point $x \in \mathbb{R}^3$.

```
ORBIT(x ∈ ℝ³)
 1  O := {x}
 2  (d, V) := DRIVER(x)
 3  while d ≠ x and x ≠ ∞ do
 4     R := ray from d in direction x
 5     y := last point behind x along R in V
 6     O := O ∪ xy
 7     x := y
 8     (d, V) := DRIVER(x)
 9  return O
```

Figure 9: The algorithm to compute the flow orbit of a given point x in $\mathbb{R}^3$.

The algorithm ORBIT successively adds line segments xy to the orbit O, which gets initialized with the point x itself. This ensures that the algorithm works correctly also in the case that x is a critical point. If x is a critical point then it is its own driver and the condition in line 3 is violated. If x is not critical and is not a point at infinity, the next line segment xy, which starts at x and ends in y, is computed in the body of the **while** loop. Note that it is indeed possible that the point y computed within this loop is a point at infinity.

Remark. The process of computing the flow orbit of a point is numerically unstable and the calculation errors can accumulated along the flow path. This can be regarded as a substantial weak-point of flow related approaches to shape ore medial axis reconstruction and analysis. Cazals [6] presents methods for carrying out these calculations robustly in 3D.

Unstable Manifolds Recall that the critical points of h_P are exactly the intersection points of Delaunay faces and their dual Voronoi faces, which we consider to be closed. It turns out that the dimension of the Delaunay face characterizes the type of the critical point: it is a local minimum if the Delaunay face is zero-dimensional, a saddle point if the Delaunay face is one- or two-dimensional and a local maximum if the the Delaunay face is three-dimensional; see [12] for more details. For a critical point we call the dimension of its corresponding Delaunay face the index of the critical point.

In order to compute the set $\mathcal{C}$ we have to compute the unstable manifolds of all medial axis critical points. Clearly, local minima, i.e., the points in P, cannot be close to the medial axis. But all other types of critical points can, and we have to consider all of them. The unstable manifold of a local maximum of h_P is just the local maximum itself, i.e., a single point. Let us now consider the unstable manifold of an index-2-saddle point.

Lemma 5.1 *Let c be an index-2-saddle point of h_P. The unstable manifold $\mathrm{Um}(c)$ of c is a piecewise linear curve. Indeed, $\mathrm{Um}(c)$ consists of the Voronoi edge $V(c)$ along with the flow orbits of its two end point.*

Proof. Note that c is the intersection point of a two-dimensional Delaunay face with its dual Voronoi edge E. We show that in a sufficiently small neighborhood U of c, $\mathrm{Um}(c) \cap U = E \cap U$. Since c is the driver of all points in the relative interior of E we have $E \cap U \subset \mathrm{Um}(c) \cap U$. It remains to show $\mathrm{Um}(c) \cap U \subset E \cap U$. Every $x \in U \setminus E$ has to be contained in interior of one of the higher dimensional Voronoi faces that contain E in their boundary. Let V be such a Voronoi face and let d be the driver of all points in the relative interior of V. By the definition of the flow ϕ_P the

```
INDEX-2-UNSTABLEMANIFOLD (c)
1  E := Voronoi edge that contains c
2  U := E
3  u, v := endpoints of E
4  if u ≠ ∞ do
5     U := U ∪ ORBIT(u)
6  if v ≠ ∞ do
7     U := U ∪ ORBIT(v)
8  return U
```

Figure 10: The algorithm for computing the unstable manifold of an index 2 saddle point.

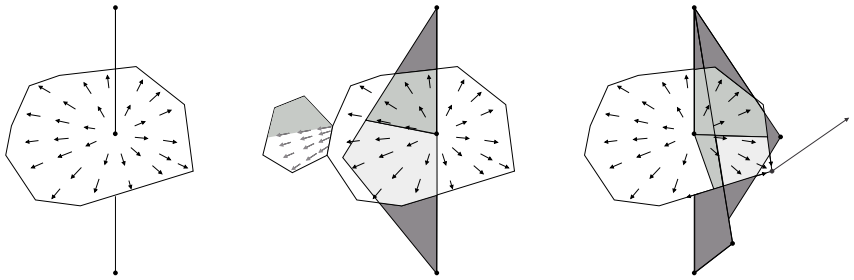

Figure 11: Left: A Voronoi face intersected by its dual Delaunay edge. The intersection point is a critical point of h_P, which drives all points in the relative interior of the Voronoi face (the arrows indicate the induced vector field). Middle: The flow continues into another Voronoi face. Note that not the whole Voronoi face has to be part of the unstable manifold. Right: The unstable of an index-2-saddle point can have one-dimensional parts, which are orbits of Voronoi vertices.

only points $y \in V$ for which $\phi_P(t, y) = x$ for some $t \geq 0$ have to reside within the intersection of V with the line segment that connects d and x. No point of the latter line segment is contained in a sufficiently small neighborhood of c, since d is a point on the boundary of the Delaunay face dual to E, whereas c is contained in the relative interior of this face. That is, $x \notin \mathrm{Um}(c) \cap U$ and thus $\mathrm{Um}(c) \cap U \subset E \cap U$. This implies that $\mathrm{Um}(c)$ is the union of E and the orbits of the endpoints of E, i.e., $\mathrm{Um}(c)$ is a piecewise linear curve. ■

Using the algorithm ORBIT, it is straightforward to construct an algorithm to compute the closure of the unstable manifold of an index-2-saddle point c. This algorithm is given in Figure 10. We will also use the algorithm ORBIT to compute the unstable manifold of an index-1-saddle point. The latter unstable manifolds are "hairy" piecewise linear surfaces. By a *hairy* surface we refer to a piece-wise linear surface to the boundary of which a finite number disjoint piece-wise linear curves (*heirs*) are attached from one end.

Lemma 5.2 *Let c be an index-1-saddle point of h_P. The unstable manifold $\mathrm{Um}(c)$ of c is the union of a piecewise linear surface and the orbits of some Voronoi vertices in the boundary of the surface.*

Proof. Ideas of this proof are visualized in Figure 11. Note that c is the intersection point of a Delaunay edge with its dual two-dimensional Voronoi face V. With a similar argument to the one given in proof of Lemma 5.1, one can show that in a sufficiently small neighborhood U of c,

$\mathrm{Um}(c) \cap U = V \cap U$. Since c is the driver of all points in the relative interior of V we have $V \subseteq \mathrm{Um}(c)$. The orbits of all points in the Voronoi edges incident to V also belong to $\mathrm{Um}(c)$. Each such Voronoi edge E falls into one of two cases: either the affine hull of E intersects its dual Delaunay face or it does not.

In the first case we distinguish two sub-cases: either E itself (not only its affine hull) intersects its dual Delaunay face or it does not. In the first sub-case, the union of the orbits of the points in E is exactly the unstable manifold of the intersection point, which is by definition a critical point. If this unstable manifold is different from E, i.e., if the endpoints of E are not critical (local maxima), then the orbits of the endpoints might be hairs of $\mathrm{Um}(c)$. In the second sub-case, it is not difficult to see that the union of the orbits of the points in E is the union of E and the orbit of one of its endpoints. The latter orbit also might be a hair of $\mathrm{Um}(c)$.

In the second case, where the affine hull of E does not intersect its dual Delaunay face, the driver d of the points in the relative interior of E is on the boundary of the Delaunay face dual to E, i.e., on a Delaunay edge and therefore is also the driver of all the points in the relative interior of the Voronoi face V' dual to the Delaunay edge. Let u and v be the endpoints of E. Since d is by definition contained in the affine hull of V' we can determine the part of V' that belongs to $\mathrm{Um}(c)$ by shooting rays from d in the direction of u and v, respectively. These rays enclose a wedge W in the affine hull of V' that contains E. We have $W \cap V' \subset \mathrm{Um}(c)$. Note that $W \cap V'$ is linear surface patch. The boundary of this patch consists of Voronoi edges or line segments contained in Voronoi edges. The orbits of all points in these edges/segments also belong to $\mathrm{Um}(c)$. We can compute the collection of these orbits recursively as a collection of surface patches and orbits of Voronoi vertices. Note that the "hairs", i.e., orbits of Voronoi vertices that are not contained in one of the surface patches, can only originate from the boundary of the surface patch and therefore, the relative interior of the unstable manifold is a two-dimensional manifold. ■

We should point out here that the hairs are topologically important. Neglecting the hairs destroys the guarantee of homotopy equivalence of $M(S)$ and the core $\mathcal{C}$. The characterization of the unstable manifolds of index-1-saddle points immediately suggests the algorithm of Figure 12 to compute them.

Unstable Flow Complex As shown above, the unstable manifold of a critical point can be seen as a piece-wise linear cell complex. Each cell of such a complex is the intersection of the unstable manifold in question and some Voronoi cell. However, since unstable manifolds of two (or more) critical points can have non-empty intersections, the union of the cell-complexes that form individual unstable manifolds does not necessarily result in a properly embedded cell-complex. This is because many cells in this union may overlap. The unstable flow complex as defined in Section 2 is a natural way to cleanly resolve this issue.

Every regular point x on the 2-skeleton of $\mathrm{Vor}(P)$ is in the unstable manifolds of at least two critical points since it is obviously contained in the unstable manifolds of all the minima in $A_P(x)$. On the other hand, the points in the interior of any Voronoi cell V_p of a point $p \in P$ are only contained in the unstable manifold of the minimum p (note that every sample point is a minimum of the distance function). This implies that the interior points of V_p, i.e., points that are strictly closer to p than to any other point in P form the cell of $\mathbf{U}$ associated to the singleton set $\{p\}$ of critical points and that these are the only cells of $\mathbf{U}$ that are associated to singletons. In other words, the 3-cells of $\mathbf{U}$ coincide with those of $\mathrm{Vor}(P)$ and therefore the rest of the cells of $\mathbf{U}$, are contained in the 2-skeleton of $\mathrm{Vor}(P)$. Indeed these cells subdivide the 2-skeleton of $\mathrm{Vor}(P)$ and the problem of computing the unstable flow complex of P boils down to computing this subdivision. This subdivision can be trivially achieved through computing individual unstable manifolds, as

```
INDEX-1-UNSTABLEMANIFOLD (c)
 1  F := Voronoi face that contains c
 2  U := F
 3  Q := ∅
 4  for each Voronoi edge E = vw incident to
F do
 5     Q.push(E, v, w)
 6  while Q ≠ ∅
 7     (E, v, w) := Q.pop()
 8     (d, V) := DRIVER((v + w)/2)
 9     if E ⊂ V do
10        compute wedge W from v, w and d
11        U := U ∪ (W ∩ V)
12        push all triples (E', v, w') ≠ (E, v, w)
for
          maximal line segments v'w' in the
          boundary of W ∩ V onto Q
13     else
14        U := U ∪ E ∪ ORBIT(v) ∪ ORBIT(w)
15  return U
```

Figure 12: The algorithm for computing the unstable manifold of an index 1 saddle point.

follows: start with the 2-skeleton of $\mathrm{Vor}(P)$ as $\mathbf{U}$ and iterate over the critical points of index 1 or higher, in an arbitrary order. For each such critical point c, compute the unstable manifold $\mathrm{Um}(c)$ and subdivide along the boundary of $\mathrm{Um}(c)$, the cells of the current complex $\mathbf{U}$ that are partially contained in $\mathrm{Um}(c)$.

Flow Closures and Flow DAG The unstable flow complex $\mathbf{U}$ can be used to compute the flow closure of a collection of its cells. For a face f of $\mathbf{U}$, it is easy to compute the set of all points that can be reached from f under the flow. An important property of $\mathbf{U}$, directly derived from its definition, is that if the flow orbit $\phi_P(t, x)$ of a point x of a face f of $\mathbf{U}$ flows into a neighboring face f', then every point of f' can be reached from some point of f under the flow. In other words, every face of $\mathbf{U}$ flows into a set of whole faces. Thus, in computing the flow closure of a face, no other face needs to be subdivided—notice that this is not the case for all faces of the Voronoi 2-skeleton (though it is the case for the faces that contain a critical point). Consequently, one can construct a *flow graph* $\mathcal{F}$, a directed acyclic graph (DAG), whose vertices are the faces of the unstable flow complex and two vertices f and f' are connected by an oriented edge if the face of $\mathbf{U}$ corresponding to f is incident to and flows into the one corresponding to f'. Given this graph, the unstable manifold of a critical point c can be easily computed by locating the corresponding face of $\mathbf{U}$, and finding all the faces of $\mathbf{U}$ whose corresponding vertices in $\mathcal{F}$ are reachable from that of c. The core $\mathcal{C}$ of the medial axis can thus be computed as the set of all faces of $\mathbf{U}$ whose corresponding vertices in $\mathcal{F}$ are reachable from some vertex of $\mathcal{F}$ corresponding to a face of $\mathbf{U}$ containing a medial axis critical point.

The complex $\mathbf{U}$ also allows us to compute the flow closure of any collection of its faces. Since $\mathbf{U}$ is a refinement of $\mathrm{Vor}(P)$ it enables us to compute the flow closure of any face of $\mathrm{Vor}(P)$ by simply

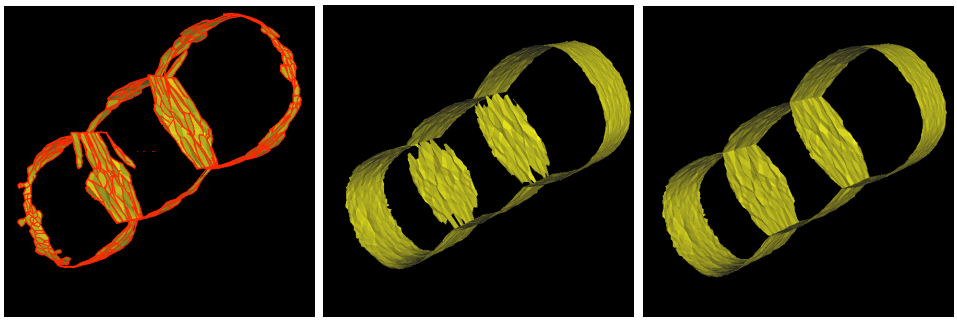

Figure 13: Left: Core computed for the 3-holes model. The red lines are either unstable manifolds of index-2 saddle points or the one dimensional parts (hairs) of the unstable manifold of index-1 saddle points. Middle: Filtered Voronoi facets based on a condition similar to the angle condition of Dey and Zhao. Right: Extended core, i.e., the core, plus the flow closures of the facets from the middle picture.

taking the union of flow closures of the faces of $\mathbf{U}$ that are contained in the given face of $\mathrm{Vor}(P)$. Computing the flow closure of Voronoi facets is useful to transfer the topological guarantees that we provide in this paper to algorithms that approximate the medial axis geometrically well by picking certain Voronoi facets, e.g., the facets picked by the medial axis approximation algorithm of Dey and Zhao [10]. In their paper Dey and Zhao show that the facets they pick are close to the medial axis provided the sampling P is sufficiently dense.

6 Experiments and Conclusion

We introduced the notion of the *core* of a medial axis approximation as the union of unstable manifolds of medial axis critical points of the distance to a sampling of a surface. If the sampling is dense enough the core is homotopy equivalent to the shape enclosed by the sample surface. We further showed how the core can be augmented to turn many medial approximation algorithms into topologically accurate ones. Finally we showed that the core and related flow closures converge to subsets of the medial axis when the input sample grows infinitely dense.

Figure 13 shows one result obtained with an implementation of the unstable flow complex data structure, the core, and the extension of the core using Voronoi facets filtered using conditions similar to those in [10]. As can be observed, the flow closure has filled the holes in the junctions of the geometric approximation of the medial axis with filtered Voronoi facets.

Acknowledgments The authors would like to thank Bálint Miklós and Jingyi Jin for the implementation and the presented output pictures.

References

[1] Nina Amenta and Marshall W. Bern. Surface reconstruction by voronoi filtering. *Discrete & Computational Geometry*, 22:481–504, 1999.

[2] Nina Amenta, Marshall W. Bern, and David Eppstein. The crust and the β-skeleton: Combinatorial curve reconstruction. *Graphical Models and Image Processing*, 60(2):125–135, 1998.

[3] Dominique Attali, Jean-Daniel Boissonnat, and Herbert Edelsbrunner. Stability and computation of the medial axis — a state-of-the-art report. *Mathematical Foundations of Scientific Visualization, Computer Graphics, and Massive Data Exploration*, 2004.

[4] Nina Amenta, Sunghee Choi, and Ravi Krishna Kolluri. The power crust, unions of balls, and the medial axis transform. *Computational Geometry*, 19(2-3):127–153, 2001.

[5] Jean-Daniel Boissonnat and Frédéric Cazals. Smooth surface reconstruction via natural neighbour interpolation of distance functions. *Computational Geometry*, 22(1-3):185–203, 2002.

[6] F. Cazals. Robust construction of the extended three-dimensional flow complex. Research Report 5903, INRIA, 2006.

[7] Tim Culver, John Keyser, and Dinesh Manocha. Exact computation of the medial axis of a polyhedron. *Computer Aided Geometric Design*, 21(1):65–98, 2004.

[8] Frédéric Chazal and André Lieutier. The λ-medial axis. *Graphical Models and Image Processing*, 67(4):304–331, 2005.

[9] Tamal K. Dey, Joachim Giesen, Edgar A. Ramos, and Bardia Sadri. Critical points of the distance to an epsilon-sampling of a surface and flow-complex-based surface reconstruction. In *Symposium on Computational Geometry (SCG)*, pages 218–227, 2005.

[10] Tamal K. Dey and Wulue Zhao. Approximating the medial axis from the voronoi diagram with a convergence guarantee. *Algorithmica*, 38:179–200, 2003.

[11] Herbert Edelsbrunner and Ernst P. Mucke. Simulation of Simplicity: A Technique to Cope with Degenerate Cases in Geometric Algorithms. In *Symposium on Computational Geometry (SCG)*, pages 118–133, 1988.

[12] Joachim Giesen and Matthias John. The flow complex: A data structure for geometric modeling. In *Symposium on Discrete Algorithms (SODA)*, pages 285–294, 2003.

[13] Karsten Grove. Critical point theory for distance functions. *Symposia in Pure Mathematics*, 54(3):357–385, 1993.

[14] Allen Hatcher. *Algebraic Topology*. Cambridge University Press, 2001.

[15] M. John. *Flow Complexs: Structure, Algorithms, and Applications*. PhD thesis, Swiss Federal Institute of Technology, ETH Zürich, 2003.

[16] André Lieutier. Any bounded open subset of $\mathbb{R}^n$ has the same homotopy type as its medial axis. *Computer-Aided Design*, 36(11):1029–1046, 2004.